PHILOSOPHICAL MAGAZINE B, 1991, VOL. 63, NO. 4, 867–890

On the formation of twinned precipitates in Al–Ge alloys

By J. DOUIN†, U. DAHMEN and K. H. WESTMACOTT

National Center for Electron Microscopy, Materials Sciences Division,
University of California, Lawrence Berkeley Laboratory,
Berkeley, California 94720, U.S.A.

(*Received 1 December 1989‡ and accepted 30 April 1990*)

ABSTRACT

High-resolution microscopy has been used systematically to obtain a detailed understanding of the morphologies and substructures of Ge needle or lath precipitates in an Al–Ge alloy. We show that the many orientation relationships observed in twinned ⟨100⟩ and ⟨110⟩ needles can be related to only three basic lattice correspondences. The feature common to ⟨100⟩ and ⟨110⟩ needles is the arrangement of five cozonal twin segments whose relative degree of development determines the cross-section morphology. Proposed growth mechanisms based on multiple twinning can account for the formation of all the different observed precipitate morphologies and defect substructures. The central role of twinning and the critical need for vacancies during nucleation are discussed in terms of possible models for nuclei that maximize the number of Ge–Ge bonds through twinning and thus minimize the need for vacancies.

§1. INTRODUCTION

Al–Ge and Al–Si alloys are metallurgically simple. Both form eutectics and have limited and strongly temperature dependent Al-rich terminal solid solubilities which gives rise to classical age-hardening behaviour. In both systems an appropriate quenching-and-ageing treatment results in direct precipitation of the equilibrium pure Ge or Si phase without intermediate phase formation. In contrast with their simple phase diagrams, however, the morphology of the precipitate structures as determined by transmission electron microscopy (TEM) studies is surprisingly complex (Saulnier 1961, Köster 1969, 1971, Gouthama, Subbanna and Kishore 1985, Gouthama and Kishore 1987, Hugo and Muddle 1986, Westmacott and Dahmen 1986, 1987). Al–Si alloys form plate, needle and lath precipitates on various habits (Saulnier 1961, Westmacott and Dahmen 1985) while in Al–Ge alloys similar morphologies but sometimes different habits have been reported (Köster 1969, 1971, Hugo and Muddle 1986, 1989). Several different orientation relationships (ORs) were determined in most of the investigations but the results were generally consistent. A common feature of the observations was the occurrence of twinning in the precipitate particles (Köster, 1969, Gouthama *et al.* 1985, Gouthama and Kishore 1987, Dahmen and Westmacott 1986).

In many respects, Al–Ge and Al–Si are ideal model systems for studying precipitation, and some aspects, particularly nucleation, have been investigated in

† Present address: ONERA, BP72, 92322 Châtillon Cedex, France.
‡ Received in final form 12 April 1990.

detail (Rosenbaum and Turnbull 1958, 1959, Lorimer and Nicholson 1969, Russell 1969, Ozawa and Kimura 1970, Beller 1972, Westmacott and Dahmen 1987). This work has verified the indispensable role of vacancies in the nucleation and growth processes. However, a detailed understanding of precipitation in these systems is hindered by the formidable obstacle of explaining how at the atomic scale the relatively open Ge and Si diamond cubic structures can form and grow in the close-packed Al f.c.c. matrix. In the present contribution a systematic atomic-resolution microscopy study of needle- and lath-shaped precipitate morphologies and substructure in an Al–Ge alloy was conducted to elucidate the role of twinning in precipitate nucleation and growth.

§2. Orientation relationships

Precipitation in Al–Ge, and also Al–Si, is noted for the variety of different ORs that are observed, and a summary has been compiled in the table. Although ORs are uniquely described in terms of a pair of parallel planes and a pair of parallel directions in that plane, three orthogonal pairs of parallel directions are given in the table for completeness. Since both crystals are cubic, directions and plane normals are identical, and the usual brackets indicating planes or directions have been omitted. For clarity, specific indices (e.g. $1\bar{1}1$) rather than general (e.g. 111) have been used to show that the three pairs of indices used to describe each OR form an orthogonal set. Any such orthogonal set can of course be replaced with a crystallographically equivalent one.

One of the predominant precipitate morphologies in Al–Ge is the needle or rod precipitate which grows with a large aspect ratio. High-resolution TEM observations (Dahmen and Westmacott 1986b) have shown that these precipitates have a $\langle 110\rangle_{Ge}$ direction accurately parallel to $\langle 100\rangle_{Al}$ along the needle axis and that they invariably display internal twinning.

2.1. *⟨100⟩ precipitates*

A simple way to illustrate systematically the possible ORs for ⟨100⟩ needles is shown in fig. 1 where four different ORs are seen as the relative rotation of one polygon within another. The truncated square represents the symmetry of the Al matrix in ⟨100⟩ projection while the inscribed truncated rectangle represents the symmetry of the Ge precipitate in ⟨110⟩ projection. Thus this figure illustrates those precipitates that have a fourfold 100 symmetry axis in Al accurately parallel to a twofold 110 symmetry axis in Ge, an alignment that was in fact found in most of the particles examined. Note that owing to this alignment ($100_{Al}\|110_{Ge}$) the two crystals share a common 2/m symmetry along the axis of these needles and the OR is at a symmetry-dictated extremum (Cahn and Kalonji 1981).

One may now imagine the precipitate crystal rotating freely inside the matrix around this common axis which it can do without destroying the common 2/m symmetry in this zone. At some special angles of rotation, further symmetry elements will come into coincidence. Four such special ORs, all based on the common twofold axis, are seen in fig. 1. Figure 1 (*a*) shows the alignment with the highest degree of symmetry. From here the other ORs, shown in figs. 1 (*b*)–(*d*), can be reached by a rotation of 45, 35·27 and 9·74° respectively. The latter two have $1\bar{1}1$ of Ge parallel to either 001 or 011 of the Al. Note that these are alignments of symmetry axes with no common symmetry elements and do not therefore represent symmetry-dictated extrema.

Summary of the different ORs of Ge or Si precipitates in an Al matrix found in the literature: DDW, present work; DNW, Dahmen, Nelson and Westmacott (1986); DW, Dahmen and Westmacott (1986a); DWb, Dahmen and Westmacott (1986b); G, Gouthama (1989 private communication); GK, Gouthama and Kishore (1987); H, Hugo and Muddle (1986); K, Köster (1969); KSO, Kobayashi, Shingu and Ozaki (1976); LH, Lu and Hellawell (1987); S, Saulnier (1961); WD, Westmacott and Dahmen (1982, 1987). The observed precipitate morphologies are indicated.

Morphology	OR		Reference	Figure
Plate on $\{111\}_{Al}$	$\bar{1}11 // \bar{1}11_{Al}$ $110 // 110_{Al}$ $1\bar{1}2 // 1\bar{1}2_{Al}$	Ge, Si	S, K, WD, GK	4(*a*)
Hexagonal plate on $\{111\}_{Al}$	$\bar{1}11 // \bar{1}11_{Al}$ $211 // 110_{Al}$ $01\bar{1} // 1\bar{1}2_{Al}$	Ge	H, G	
Plate on $\{001\}_{Al}$	$\bar{1}11 // 001_{Al}$ $110 // 110_{Al}$ $1\bar{1}2 // 1\bar{1}0_{Al}$	Ge	K, GK	4(*c*)
Plate on $\{001\}_{Al}$	$111 // 100_{Al}$ $01\bar{1} // 010_{Al}$ $\bar{2}11 // 001_{Al}$	Ge	K, G	1(*c*)
Plate on $\{001\}_{Al}$	$110 // 100_{Al}$ $001 // 001_{Al}$ $1\bar{1}0 // 100_{Al}$	Ge	GK	1(*a*)
Needle along $[100]_{Al}$	$110 // 100_{Al}$ $-1\bar{1}1 // 001_{Al}$ $\bar{1}12 // 010_{Al}$	Ge, Si	K, DNW, GK	1(*c*)
Needle along $[100]_{Al}$	$110 // 100_{Al}$ $1\bar{1}0 // 011_{Al}$ $001 // 01\bar{1}_{Al}$	Ge	H, DWb	1(*b*)
Needle along $[100]_{Al}$	$110 // 100_{Al}$ $001 // 001_{Al}$ $1\bar{1}0 // 100_{Al}$	Ge	DWb, DDW, K	1(*a*)
Needle along $[100]_{Al}$	$110 // 100_{Al}$ $1\bar{1}1 // 01\bar{1}_{Al}$ $\bar{1}12 // 011_{Al}$	Ge	DWa	1(*d*)
Lath along $[100]_{Al}$	$\bar{1}11 // 001_{Al}$ $110 // 100_{Al}$ $1\bar{1}2 // 010_{Al}$	Ge	H	1(*c*)
Needle along $[110]_{Al}$	$110 // 110_{Al}$ $\bar{1}11 // 1\bar{1}1_{Al}$ $1\bar{1}2 // \bar{1}12_{Al}$	Ge	DDW	4(*a*)
Needle along $[110]_{Al}$	$110 // 110_{Al}$ $1\bar{1}1 // 1\bar{1}2_{Al}$ $\bar{1}12 // \bar{1}11_{Al}$	Ge	H, DDW	1(*b*)
Needle along $[110]_{Al}$	$110 // 110_{Al}$ $001 // \bar{1}11_{Al}$ $1\bar{1}0 // 1\bar{1}2_{Al}$	Si	WD	4(*c*)
After eutectic solidification	$001 // 110_{Al}$ $100 // 11\bar{1}_{Al}$ $010 // 112_{Al}$	Si	KSO, LH	1(*c*)
After eutectic solidification	$11\bar{1} // 01\bar{1}_{Al}$ $112 // 111_{Al}$ $\bar{1}10 // \bar{2}11_{Al}$	Si	LH	

Fig. 1

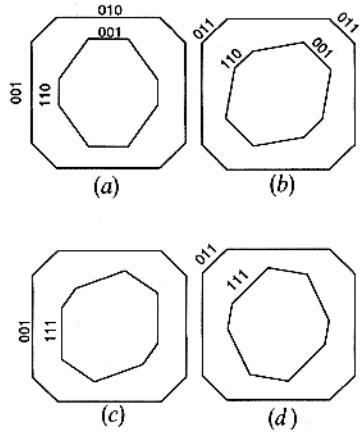

Schematic illustration of four different ORs found in Al–Ge alloys. The truncated square represents the Al matrix in ⟨100⟩ projection while the inscribed truncated rectangle stands for the Ge precipitate in ⟨110⟩ projection.

Fig. 2

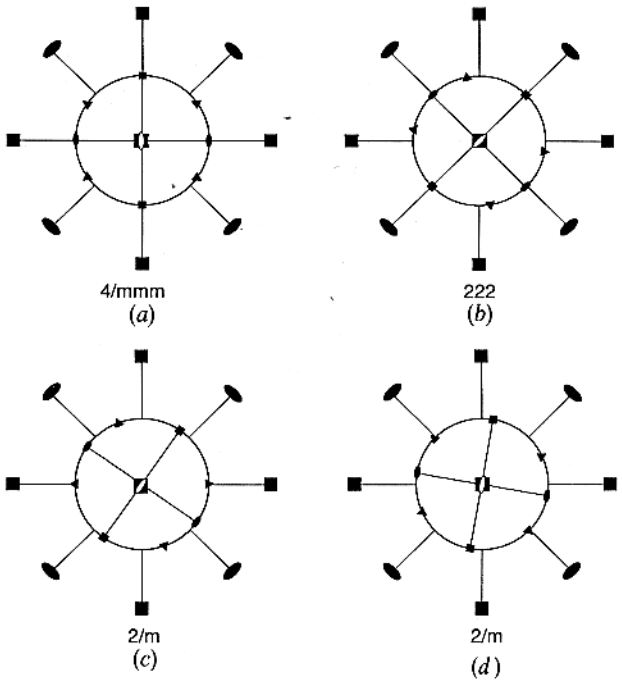

Same ORs as in fig. 1. The symmetry elements are indicated by conventional symbols.

A more accurate way of illustrating the ORs in fig. 1 is the stereographic representation in fig. 2. The symmetry elements are indicated by conventional symbols: rotation axes by twofold, threefold and fourfold symbols and vertical mirror planes by solid lines. The matrix orientation is fixed and the precipitate orientation, given by the inscribed circle, is variable. It is now easy to see the symmetry of the OR for each case. Figure 2(*a*) displays tetragonal 4/mmm symmetry, fig. 2(*b*) shows orthorhombic 222

and figs. 2(*c*) and (*d*) exhibit only the monoclinic symmetry of the common rotation axis since the alignment of a triad with an evenfold axis does not lead to any shared symmetry elements. However, these ORs do become special when twinning is taken into account.

2.2. *Twinning*

Because of the extensive twinning observed in Ge and Si precipitated not only from the bulk but also on alloy surfaces, and in pure materials during eutectic solidification, it is important to separate precipitate orientations that are mutually related by internal twinning from those that are truly distinct from each other.

Internal twinning of a precipitate by reflection across a {111} plane leads to a new Ge orientation related to the primary Ge by a 70·53° rotation about a ⟨110⟩ direction in the twin plane. In the schematic representation in figs. 1 and 2 each of the rational ORs could thus generate further ORs with the same alignment of zone axes (common 2/m symmetry) by internal twinning. Primary twinning leads to a rotation of 70·53°, secondary twinning to an additional rotation of 70·53°, and so on. If twinning occurs on the other twin plane in the common zone, it will add a rotation of −70·53°. Multiple twinning is most likely to occur on both twin planes, and the primary twins on each of the two twin systems will be related to each other by twice the rotation angle. Note, however, that the two primary twins obey different variants of the same OR with the matrix; they are related to each other by a mirror reflection across the common {001} planes in fig. 1(*a*).

Similarly, because a twin plane in the Ge is parallel to a mirror plane in the Al in figs. 1(*c*) and (*d*), primary twinning on that plane will only lead to a different variant of the same OR. Thus, by twinning on a {111} plane that is parallel to a matrix mirror, a precipitate can maintain the same OR (albeit a different variant) with the matrix.

Starting from one of the special ORs in fig. 1 it is clear that none of the other special ORs can be obtained precisely by a small number of successive twinning operations. However, as shown in fig. 3, two successive twinning operations on the precipitate of fig. 1(*a*) bring it within 3·67° (38·94 − 35·27) of that in fig. 1(*c*) and vice versa. Figures 1(*b*) and 1(*d*) are similarly related to each other. Furthermore, a double-twinning operation brings the precipitate orientations of figs. 1(*a*) and (*b*) and figs. 1(*c*) and (*d*) to 6·06° (45 − 38·94) of each other. Thus, if distortions up to this magnitude (6·06°) can be accommodated, all the ORs could be present in a multiply twinned precipitate (MTPT) and could have originated from nuclei in any one of the four ORs shown in fig. 1.

Fig. 3

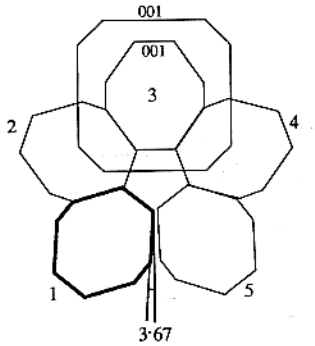

Schematic illustration of the ORs that can be obtained from that in fig. 1(*a*) (labelled 3) by multiple twinning. The OR labelled 1, reached after two successive twinning operations, is within 3·67° of the OR shown in fig. 1(*c*).

2.3. ⟨110⟩ *precipitates*

The second most common set of ORs is found in needles or laths along ⟨110⟩ directions of the matrix. Again the ⟨110⟩ direction of the precipitate is accurately aligned with its counterpart in the matrix along the needle axis. Figure 4 illustrates the possible rational ORs with this common zone axis. A stereographic representation similar to fig. 2 can be readily constructed but is omitted here for brevity.

Note that in fig. 4 (*a*) all symmetry elements are shared; this is the cube–cube OR commonly observed for plate-shaped precipitates. The OR in figs. 4 (*c*) and (*d*) have the lowest composite symmetry because they have alignments of a threefold with a twofold or fourfold axis. However, these are again important where multiple twinning is observed. Multiple twinning again brings some of the ORs close to each other. In this case, however, figs. 4 (*b*) and (*c*) and figs. 4 (*a*) and (*d*) are separated by 3·67° following a double-twinning operation on either one of the pairs, but unlike the $\langle 100 \rangle_{Al}$ needles no connection can be made between the two pairs. Thus allowing distortions up to 3·67° results in two basic orientations mutually related to two more ORs by double twinning.

Other rational ORs could be constructed in this manner, but for the purpose of classifying and discussing the experimental observations the two basic possibilities outlined above are sufficient. It is now possible to understand the connection between different ORs in the multiply twinned particles (MTPs) so frequently observed in Al–Ge and Al–Si.

§ 3. Experimental details

An alloy of nominal composition Al–1·10 at.% Ge was prepared from pure elements in the form of 0·1 mm foil. After ageing for a week at 550°C, 3 mm discs were quenched to −60°C in a solution of 75% HCl and 25% H_2O. Precipitation was ensured either by bulk or *in situ* ageing for approximately 4 h between 220 and 260°C. Thin foils were prepared by jet electropolishing using a solution of 85% methanol, 8% sulphuric acid, 5% lactic acid and 2% hydrofluoric acid between −26 and −24°C and an operating current of 28 mA.

Fig. 4

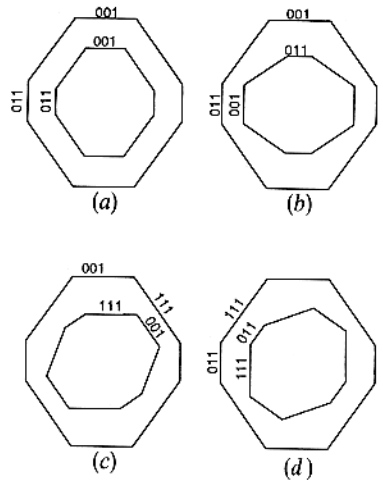

Schematic illustration of four more ORs found in Al–Ge alloys. The truncated rectangle represents the Al matrix in ⟨110⟩ projection while the inscribed truncated rectangle stands for the Ge precipitate in ⟨110⟩ projection.

In situ studies were carried out with the Kratos EM 1500 equipped with a Gatan double-tilt heating stage, and high-resolution imaging of needle cross-sections was performed using the Berkeley JEOL ARM 1000 (operating at 800 kV).

§4. Results

The overall precipitate morphology and distribution in quenched-and-aged Al–Ge is shown in fig. 5. Approximately equal densities of plate and needle precipitates are observed in both bulk aged (fig. 5 (*a*)) and thin-foil aged (fig. 5 (*b*)) specimens. In the thin-foil experiments it has been possible to examine directly the influence of vacancy supersaturation on the type of precipitate nucleated (Westmacott and Dahmen 1987).

Fig. 5

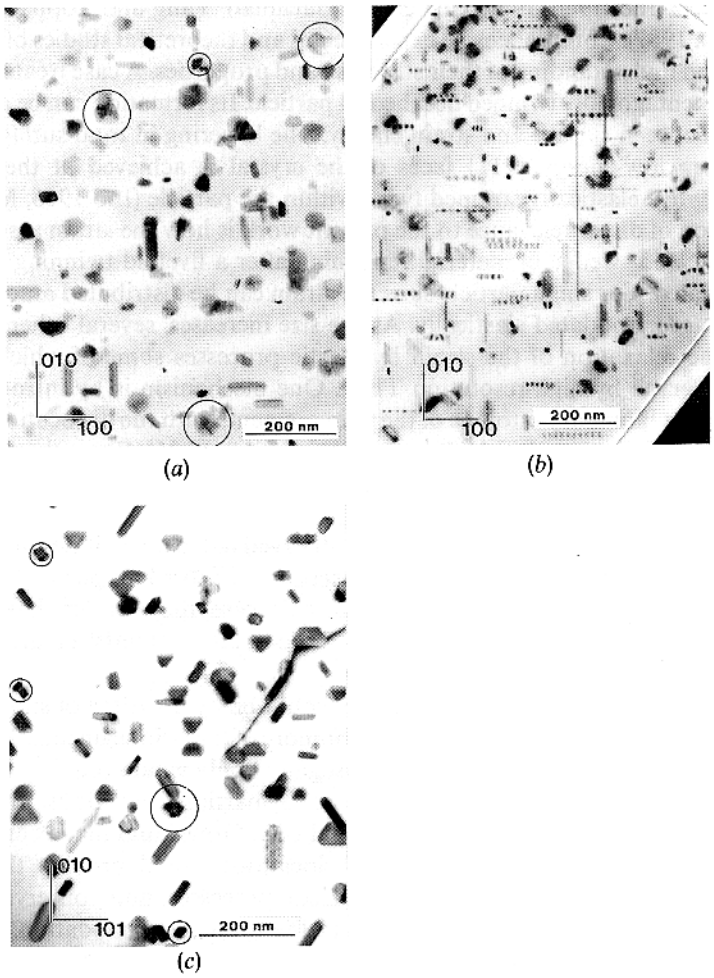

Conventional bright-field micrographs showing the morphology of Ge precipitates after (*a*), (*c*) bulk aging and (*b*) thin-foil aging. In a [001] zone axis (*a*), (*b*) the alignment of the needles along ⟨100⟩ matrix directions is apparent. Characteristic cross-sectional shapes (circled) resulting from multiple twinning of the needles are seen in $\langle 100 \rangle_{Al}$ and $\langle 110 \rangle_{Al}$ ((*a*) and (*c*) respectively). The lines with Miller indices indicate crystal directions.

It was observed that, in thin regions of a foil where substantial loss of vacancies to the surfaces occurs, needles are the predominant morphology nucleated whereas, near vacancy sources, plate precipitates are favoured. In thick regions of the foil, equal distributions of needles and plates were found similar to the structures observed in bulk aged specimens. Very long needles develop during thin-foil ageing (see fig. 5 (*b*)); this can be explained by the small mismatch between $\langle 100 \rangle_{Al}$ and $\langle 110 \rangle_{Ge}$ (about 1·2%). When viewed end on, the twinned substructure of the needles is evident even with diffraction contrast imaging. This is illustrated in fig. 5 (*c*) for $\langle 110 \rangle_{Al}$ needles with a $\langle 110 \rangle$ beam direction. Many examples of pentagonally twinned precipitates with a characteristic mushroom shape may be seen. Similar configurations, but with more symmetrical overall cross-sectional shapes, are seen for end on $\langle 100 \rangle_{Al}$ needles in fig. 5 (*a*).

Before presenting the results on the structure of twinned precipitates it is appropriate to review briefly related work on MTPs formed on substrates from the vapour phase (Ino, 1966, 1969, Heinemann, Jacamán, Yang and Poppa 1979, Marks 1984, Iijima 1987). Comprehensive experimental and theoretical studies of MTPs have led to a good understanding of their structure and properties. A case treated in detail is that of the pentagonally twinned decahedral particle. Its formation can be explained by a balance between surface and strain energy. The lowering in total surface energy by exposing ten low-energy $\{111\}$ faces of the crystal is achieved at the expense of introducing five elastically strained twins within the particle (Ino 1966, Marks 1984). The question of direct relevance to the present work is how the strain associated with the residual 7·35° wedge of material remaining after a fivefold twinning operation is accommodated. For small particle sizes the strain can be distributed amongst the five twins and accommodated elastically. As the size increases, several other possibilities exist for the relaxation of the strain by plastic processes some of which have been directly observed by high-resolution TEM. One mechanism is by introduction of a small angle tilt boundary into one of the twin segments with the dislocations spaced at intervals of $h = \theta/b$, where b is the Burgers vector and $\theta = 7{\cdot}35°$. Examples of this type of accommodation have been observed by Iijima (1987) in twinned spheres of Si crystallized from the molten state.

Another accommodation mode already observed in Ge precipitates in Al (Dahmen and Westmacott 1986a) is by the radial insertion of extra half-planes between twin segments. It is interesting to note that in this case the inserted half-planes are symmetrically disposed so as to preserve the overall symmetry of the orientation relationship.

A third method for filling the 7·35° gap would be by a variety of slip or twinning operations on the conjugate systems in one or more of the twin segments. To fill the gap completely by uniform deformation of one segment only would require the formation of a 15R polytype if the deformation took place by partial dislocations. In practice it is more likely that more than one segment would be deformed and that a combination of microtwins, stacking faults and perfect dislocations would provide the necessary deformation. In addition to conservative plastic processes, non-conservative growth mechanisms will probably also contribute to the total accommodation.

While it is useful to compare the structures of MTPs formed by vapour deposition and solid-state precipitation, the presence of a constraining matrix in the latter case will lead to differences in morphology. As pointed out earlier, the needle morphology develops by virtue of the small mismatch (transformation strain) between the $\langle 110 \rangle_{Ge}$ and the $\langle 100 \rangle_{Al}$ direction. Maintaining these alignments imposes axial symmetry on the precipitate and its substructure. It is interesting to observe how the precipitate or its

different twin segments satisfy one of the ORs with the matrix shown in figs. 1, 3 and 4. In the precipitate–matrix interfaces parallel to a needle axis, the Ge frequently exposes {111} faces to the Al matrix. However, it has been shown elsewhere (Dahmen and Westmacott 1986b) that this is only true within the constraints imposed by the symmetry of the OR.

During an *in situ* treatment, precipitates also nucleate on the surface (fig. 6), leading to a depleted layer and precipitate-free zone parallel to the surface. Their contrast indicates that they are always multiply twinned and commonly have a centre of fivefold symmetry.

A variety of cross-sectional shapes was found for both the $\langle 100 \rangle_{Al}$ and the $\langle 110 \rangle_{Al}$ needles. Interpretation of the different morphologies is based on the hypothesis that the initial nucleus is either singly twinned (Westmacott and Dahmen 1987) or pentagonally twinned (Dahmen and Westmacott 1986a) and that the possible basic ORs are those depicted in figs. 1 and 4.

4.1. *⟨100⟩ needles*

MTPTs are the most frequent configuration, and needles containing five twins along a common $\langle 110 \rangle_{Ge}$ axis can be observed after both bulk and *in situ* heat treatment. Figure 7 (*a*) shows a high resolution micrograph of the cross-section of a MTPT found in a bulk aged sample. The $\langle 110 \rangle_{Ge}$ axis of the needle is parallel to a $\langle 100 \rangle_{Al}$ direction. As already reported by Westmacott and Dahmen (1987), the facetting of the precipitate occurs mostly on $\{111\}_{Ge}$ planes and usually exhibits contrast consistent with twinning or a change in stacking sequence at the interface between the Al and Ge. Five internal twin-related segments are denoted 1–5. Segments 1 and 5 obey the OR in fig. 1 (*c*), the most commonly found OR in ⟨100⟩ needles, and make up the largest part of the precipitate. Segment 3 is relatively small, shares a common {001} plane with the Al matrix (OR in fig. 1 (*a*)) and is elastically distorted. Segment 4 is very small and strongly distorted. Since the five twins converge exactly at a point, the intersection area has a special crystallography. Figure 7 (*b*) is an enlargement of this area; the twins meet in a common centre imaged as a five-member ring of (black)

Fig. 6

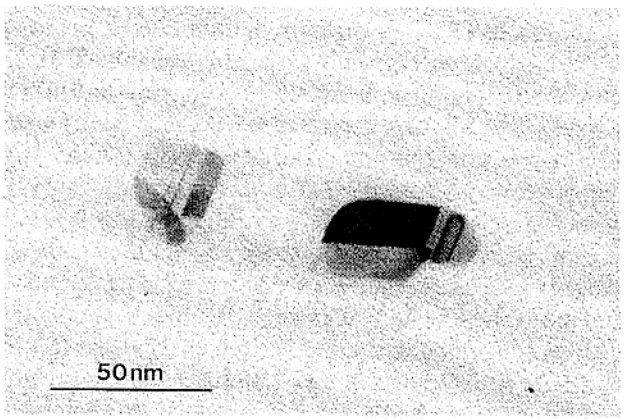

Bright-field micrograph of precipitates nucleated at the surface during *in situ* heating, showing extensive internal twinning substructure.

Fig. 7

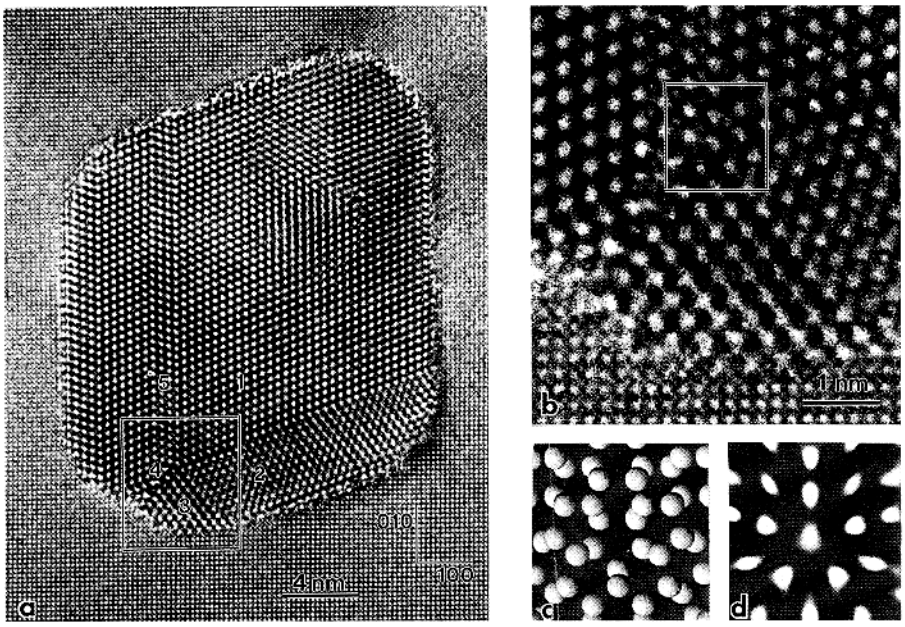

High-resolution image of a [100] needle found in a bulk aged Al–Ge alloy: (*a*) general view showing the internal structure with five twins; (*b*) enlargement of multiply twinned region of (*a*); (*c*), (*d*) model and image simulation of the five-atom ring at the intersection of the twins (thickness, 50 Å, defocus, −800 Å).

Ge atom pairs. A model of this configuration is shown in fig. 7 (*c*) and for comparison with the experimental image the corresponding image simulation in fig. 7 (*d*). This kind of ring has already been identified as the origin of the five-fold symmetry of vapour-deposited diamond particles (Matsumoto and Matsui 1983, Angus and Hayman 1988) or Si particles (Iijima 1987) and Ge precipitates (Dahmen and Westmacott 1986a). They also have been directly observed in materials with diamond or f.c.c. structure, for example during the crystallization process of amorphous Si (Li and Guo 1985) and as part of higher order twins (e.g. $\Sigma = 9$) in Ge (d'Anterroches and Bourret 1984, Skrotzki, Wendt, Carter and Kohlstedt 1988), as well as in Ag (Jefferson and Kirkland 1988).

Another example of a MTPT is given in fig. 8. Four different twin-related segments can be observed. The labelling corresponds to the notation used in fig. 7. In this particle, segment 3, which was small in fig. 7, is relatively large and undistorted. Segment 1 is negligibly small and its twin, segment 5, is relatively small as well. None of the segments shows a clear elastic distortion, but notice the alternating 2–3 and 4–5 bands of twins that appear to be correlated across the 3–4 twin boundary.

Two other types of precipitate observed in a $\langle 100 \rangle_{Al}$ zone axis are illustrated in figs. 9 and 10. Unlike the previous examples, these precipitates have a more lath-like character. Only four twin-related segments are observed in fig. 9, and the precipitate in fig. 10 is altogether untwinned. In fig. 9, segment 3 occupies the bulk of the particle. By it shape and OR the central triangular section (segment 3) at the top of this particle is easily identified with its counterparts in figs. 7 and 8. As in the previous particles this segment is flanked by its twins 2 and 4. However, instead of following these twins with segments 1 and 5 this particle reverts to twin 3. The resulting morphology is distinctly different from the preceding ones.

Fig. 8

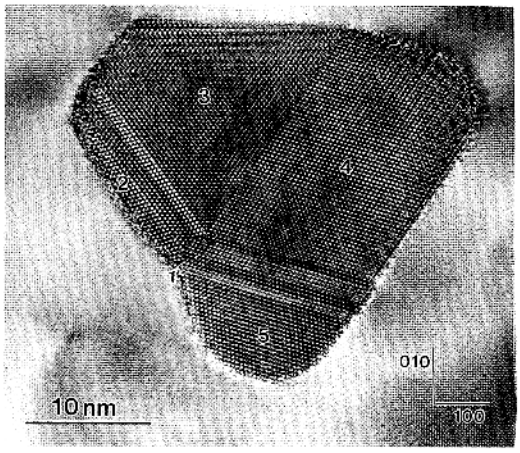

High-resolution micrograph of a MTPT with an almost triangular segment 3 and symmetrically disposed twin bands across segments 3 and 4.

Fig. 9

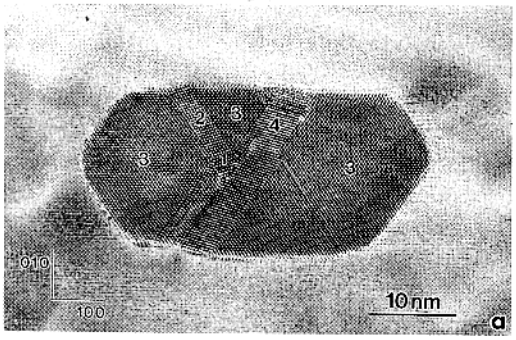

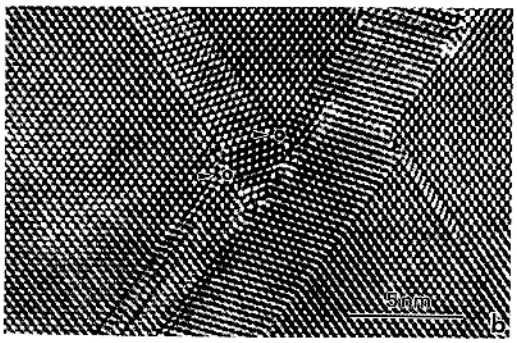

Micrograph of a precipitate with a more lath-like shape. The morphology is dominated by segment 3 and perturbed only slightly by the minor segments 1, 2 and 4.

Fig. 10

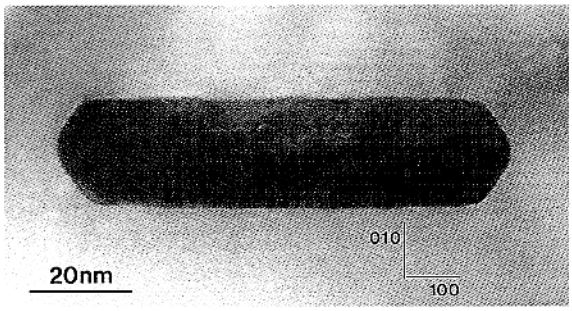

Micrograph illustrating the lath morphology of the sole example of an untwinned precipitate found in the present study.

A small piece of segment 1 is visible near the highly distorted centre of the particle and in the enlarged view shown in fig. 9 (*b*) this shows the familiar fivefold geometry (arrowed). However, this segment does not make a significant contribution to the overall particle morphology.

Figure 10 consists entirely of segment 3 and contains no twins at all. This is a relatively rare occurrence and from micrographs such as this it could not be determined whether the true shape of the particle is that of a lath or a plate. The facetting is now quite pronounced and it is interesting to note that the major facets are not of the $\{111\}_{Ge}$ type, as in vapour-deposited particles, but of the $\{100\}_{Ge}$ type with only minor $\{111\}_{Ge}$ facets at the edge of the particle.

From the examples shown in the preceding micrographs it is clear that there is a correlation between the twin substructure of a particle and its morphology. The majority of the precipitates are similar to that in fig. 7 which is dominated by the OR fig. 1 (*c*). These usually exhibit pronounced facets on $\{111\}_{Ge}$ faces that lie opposite either $\{100\}_{Al}$ or $\{310\}_{Al}$ planes. From this frequent observation it would be tempting to conclude that the morphology is determined by the same surface energy principles as that of vapour-deposited particles. However, note that segment 3 which has the OR in fig. 1 (*a*) always tends to facet on the $\{100\}_{Ge}$ face that it has common with the Al matrix, even when it is small. In contrast, segments with an OR of lower symmetry often grow to such shapes as to expose $\{111\}_{Ge}$ faces; see for example segment 4 in figs. 8 and 9. This facetting is usually not carried to the extreme of sharp corners. In fact, in all particles examined the junction of $\{111\}_{Ge}$ facets was found to be rounded off. When a segment is small such as twin 5 in fig. 8, this can result in a nearly semicircular shape.

A feature common to all $\langle 100\rangle_{Al}$ precipitates examined is the fact that all can be described as a grouping of the same five twin-related segments with different segments grown to different proportions.

Segment 3 has an outstanding role as the twin with the OR of the highest symmetry, the Bain relationship (OR in fig. 1 (*a*)). Segments 1 and 5 obey the OR in fig. 1 (*c*) which has been shown to be related (to within 3·67°) to segment 3 by secondary twinning. This small misorientation is half the angle of the missing 7·5° wedge that results when five twin segments are joined at a common apex. When several twin segments are present, the closure of this wedge angle appears to pose a problem. The parallel twin lamellae

seen in fig. 9 and the distortion of the smallest segments seen in fig. 7 are related to this wedge angle.

The most perfect example of a pentagonally twinned particle was shown elsewhere (Dahmen and Westmacott 1986a). In this precipitate the 7·5° wedge angle was filled by symmetrical radial insertion of extra half-planes on the boundaries between segments 1–2 and 4–5.

4.2. *⟨110⟩ needles*

In an analogous manner to $\langle 100\rangle_{Al}$ needles, $\langle 110\rangle_{Al}$ needles also display several different morphologies. Because in both cases the needle axis lies along a $\langle 110\rangle_{Ge}$ direction it is again possible to resolve the substructure, morphology and OR in high-resolution micrographs that show the needle structure in cross-section. Several representative particles are described in this section. All observed ORs can be rationalized, and the different twin segments are labelled, with reference to fig. 4.

It is evident from an examination of the low-magnification micrograph in fig. 5 (*c*) that $\langle 110\rangle_{Al}$ needles frequently exhibit pentagonal twinning. Such precipitates have a characteristic 'mushroom' shape as illustrated in figs. 11 and 12. Segment 3 in figs. 11 and 12 exhibits the cube–cube relationship (OR in fig. 4 (*a*)) while segment 2 follows the cube–twin OR. The main difference between the two particles in figs. 11 and 12 lies in the degree of development of segments 4 and 5 and the substructure of parallel twin bands. Segments 4 and 5 are well developed in fig. 11 and the parallel twin bands are of the type 4–3 and 1–5. In fig. 12, segments 4 and 5 are both equally undeveloped and thin parallel twin bands are of the type 1–2 and 3–4. Figure 12 (*b*) is an enlargement of the region in which the five twins intersect. The convergence of the five twin segments in a common centre is clearly visible. The twin boundaries are marked with arrows and because in this region all twins meet coherently on $\{111\}_{Ge}$ planes they must be elastically distorted to close the 7·5° wedge angle.

Figures 13 (*a*) and (*b*) are two examples of needles that at first sight appear to display no rational OR with the matrix. However, closer inspection shows that segment 4 in

Fig. 11

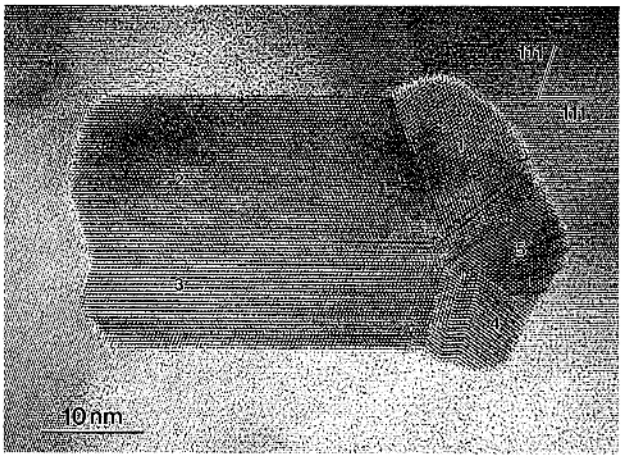

High-resolution micrograph of a $\langle 110\rangle_{Al}$ needle with the so-called mushroom configuration. Most of segment 3 has the cube–cube OR in fig. 4 (*a*). The multiply twinned end appears to have pseudo-fivefold symmetry.

Fig. 12

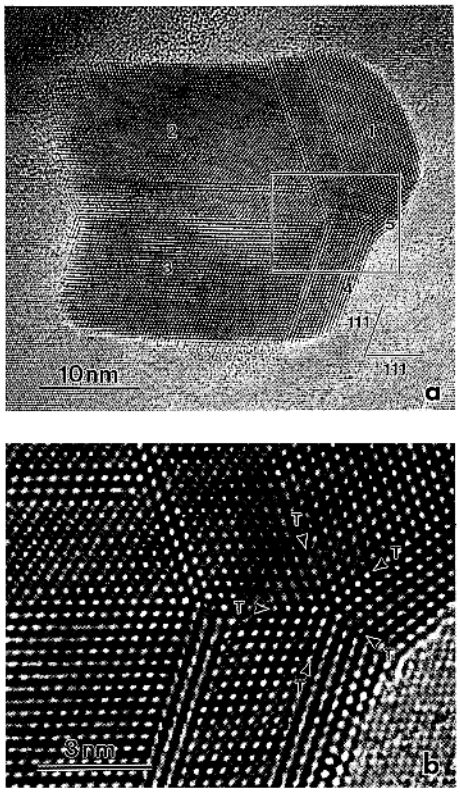

High-resolution micrograph of another example of a $\langle 110 \rangle_{Al}$ mushroom needle; (*b*) enlargement showing clearly that the intersection of five twins, the boundaries of which are marked T, leads to a five-atom ring of Ge.

fig. 13 (*a*) is related to the OR depicted in fig. 4 (*d*) by tertiary twinning and segment 5 by quaternary twinning (see fig. 13 (*c*)). In fig. 13 (*b*), segments 2 and 3 are related to the OR in fig. 4 (*b*) by primary and secondary twinning respectively, as shown in fig. 13 (*d*). Thus each case is related to a primary OR by a sequence of twinning operations.

The morphology of the $\langle 110 \rangle_{Al}$ needles is quite similar to that of $\langle 100 \rangle_{Al}$ needles; the external shape is related to the internal defect substructure by a tendency for facetting on $\{111\}_{Ge}$ planes. This leads to V-shaped notch on the thin end of the 'mushroom' morphology. The tendency towards $\{111\}_{Ge}$ facets is clearly most pronounced for segments 2 and 3 which have an OR with high symmetry. Most other segments are rounded, possibly owing to their smaller size.

§ 5. Discussion

5.1. *Importance of twinning*

The results shown in the preceding sections illustrate the great variety of ORs and morphologies that are observed in quenched-and-aged Al–Ge alloys. Throughout the presentation of the experimental results the relationship between the twin substructure of a precipitate and its morphology has been emphasized. Twinning appears to be present at least once in almost every precipitate and it is clear that twinning is

Fig. 13

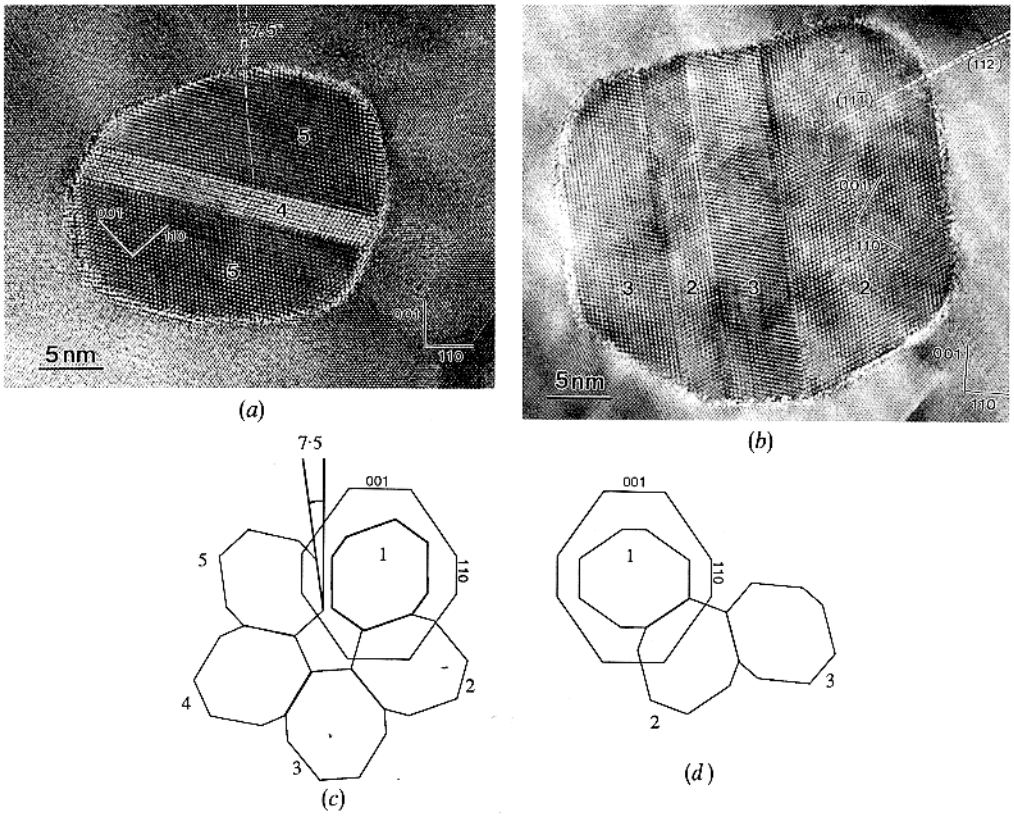

(*a*), (*b*) High-resolution micrographs of two other ORs commonly found in $\langle 110 \rangle_{Al}$ needles. The ORs observed are related to those in figs. 4 (*d*) and (*b*) by multiple twinning as illustrated schematically in (*c*) and (*d*) for (*a*) and (*b*) respectively.

intimately related to nucleation and growth. This is true for the observations on needle-shaped precipitates presented here as well as for plate-shaped precipitates examined previously. Very similar results are found for Al–Si alloys which exhibit the same spectrum of morphologies and the same ubiquitous twinning. Furthermore, a comparison between the substructures of $\langle 100 \rangle_{Al}$ and $\langle 110 \rangle_{Al}$ needles shows that fivefold twinning appears to play a special role. It is interesting to see that the bewildering variety of ORs can be related to just three basic relationships through multiple-twinning operations.

The Ge frequently exposes {111} faces to the Al matrix, as is found in vapour-deposited particles. However, because of the OR with the surrounding matrix, equivalent {111} faces of the Ge will often see non-equivalent faces in the Al. In well developed particles with equilibrium shapes, {111} facetting is therefore found only within the constraints imposed by the composite symmetry of the OR (Cahn and Kalonji 1981), and precipitates with high-symmetry ORs often display large {100} or {110} facets. Furthermore the observed precipitates do not approximate spheres, as in vapour deposited decahedral or icosahedral particles, but needles or laths. Where they are bounded by {111} faces these are parallel to the needle axis rather than inclined as in a decahedron.

5.2. *Lattice correspondence*

The fact that ORs are observed at all implies some interaction between the Al matrix and the Ge precipitates that makes crystal alignments preferable to random orientation. However, it is difficult to find a reasonable lattice correspondence between the f.c.c. Al and the diamond cubic Ge lattice. Because the motif of the diamond cubic lattice has twice the number of atoms of the fc.c. lattice, two unit cells of the Al lattice must correspond to one cell in the Ge lattice for a conservative lattice correspondence (conserving the number of lattice sites). The simplest way of accomplishing this is the correspondence shown in fig. 14 (*a*), which is similar to the Bain correspondence in the f.c.c.–b.c.c. case; the lattices are aligned along a common cube axis and rotated by 45° relative to each other about that axis. The transformation strain is relatively small and uniform in the common cube face: $a_{Ge}/\sqrt{2}a_{Al}=0{\cdot}989$. On the other hand, along the common cube direction, the strain is large: $a_{Ge}/a_{Al}=1{\cdot}399$. The principal distortions of the transformation strain matrix are thus (0·989, 0·989, 1·399) when referred to the cube axes of the Al matrix. However, owing to the large 36% volume increase, precipitation without vacancies is not possible. It has been found repeatedly and reproducibly that precipitate-free zones form near grain boundaries and other vacancy sinks. Vacancies may thus be thought of as an integral part of any operating lattice correspondence. One suggestion has been the incorporation of as many as 50% vacancies in a lattice correspondence with the same relative lattice orientation as that described above (A. G. Khachaturyan 1986 private communication). If half of the atoms in each {001} layer are replaced by vacancies, two Al unit cells will collapse to one diamond cubic unit cell (see fig. 14 (*b*)). The transformation strains would then be (0·989, 0·989, 0·699).

These two extreme cases since one lattice correspondence incorporates substantially more vacancies (50%) than required for complete volume accommodation (36%), and the other one none at all (conservative). In either case appreciable strain will have to be accommodated by lattice deformation, an expansion for the conservative case and a contraction for the non-conservative case with 50% vacancies.

Fig. 14

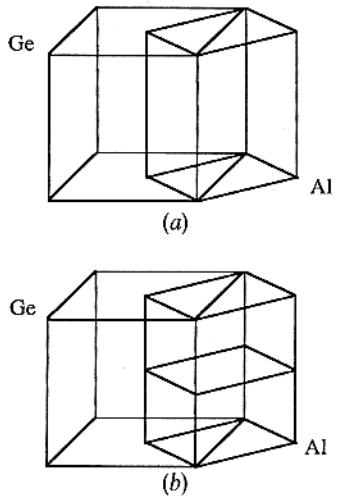

Diagrams showing (*a*) a conservative Bain lattice corresponding requiring an expansion of the Al matrix and (*b*) an alternative non-conservative Bain correspondence requiring the incorporation of 50% vacancies in the lattice.

Other lattice correspondences can be searched out with the aim of incorporating close to the required number of vacancies and thus minimizing the accommodation strain. This is the procedure followed in the near-coincidence-site lattice (CSL) approach, usually applied to two- dimensional interfaces (Zur and McGill 1983, Gao, Shewmon and Dregia 1988) but easily extended to three dimensions. The aim here is to find a near-CSL cell that is small enough to have physical significance and incorporates nearly the required number of vacancies thus needing only small transformation strains. For Al–Ge, one such correspondence is that shown in fig. 15. If the two lattices are in a parallel (cube–cube) OR, then a near coincidence is established every seven spacings (five Ge spacings). This is commonly denoted as $\Sigma = 5/7$, and in three dimensions becomes $\Sigma = 125/343$. The residual strain is minimal (0·1%), compared with the largest strain of the conservative correspondence (39·9%). However, the number of atoms in such a coincidence cell is large, that is only one in every 343 Al atoms (250 Ge atoms) is related in this way (as opposed to one in two atoms for the case of the conservative correspondence).

In actual precipitate growth an interesting variation on this principle is found; Si plates that form in cube–cube OR on {111} planes of the Al matrix assume the planar near-CSL lattice correspondence in the habit plane but maintain a one-to-one correspondence normal to the habit plane. This is evident from the strain contrast that develops as the plates thicken. A ⟨110⟩ interstitial strain field similar to that of a prismatic dislocation loop builds up until it is relieved by the precipitation of a layer of vacancies (Westmacott and Dahmen 1987). A point of interest about this observation is that the developing strain field has a shear component parallel to the habit plane; therefore it could exert a bias on subsequent twin formation. The implications of this will be discussed in § 5.3.

Another possible lattice correspondence is shown in fig. 16. This is designated as the inverse Bain correspondence. Here the mismatch along the common ⟨110⟩ direction is large and that in the common {110} plane is small.

Many other possible near-CSL orientations and lattice correspondences could be found by using a computer algorithm (Zur and McGill, 1983, F. R. Chen 1988, private communication). However, since no criteria for optimization have been established, the usefuness of such an exercise is doubtful without further reference to experimental observation.

A common factor in all needle and lath morphologies is the perfect lattice alignment along the needle axis as opposed to the many different orientations about this common

Fig. 15

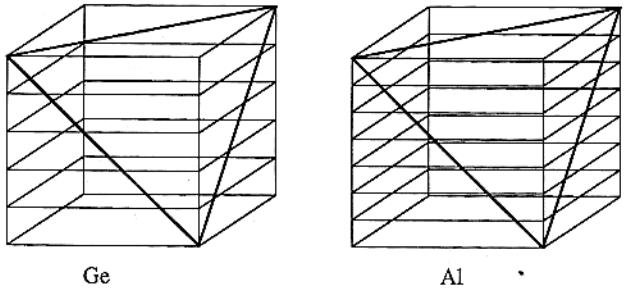

A near-CSL ($\Sigma = 125/343$) for a cube–cube lattice correspondence reflects the close atomic match indicated for one set of cube planes between seven Al and five Ge spacings.

Fig. 16

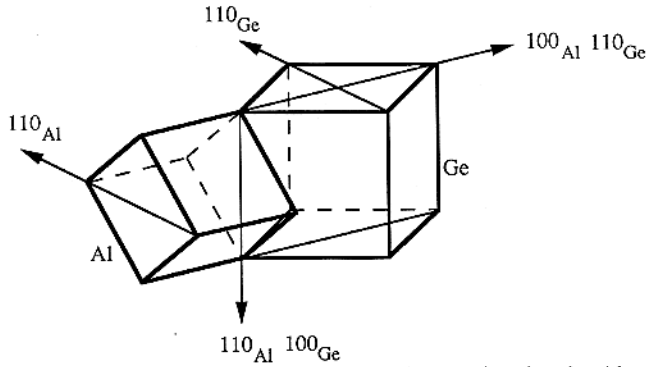

Diagram illustrating the inverse Bain lattice correspondence whereby the Al and Ge lattices share a common ⟨110⟩ direction.

zone. Close inspection of the contrast behaviour of the precipitates confirms this difference; along the needle axis there is evidence of dislocations and localized strains whereas no dislocations could ever be identified in any of the high-resolution images of cross-sections viewed along the needle axis. The absence of dislocations in the cross-sectional images is in contrast with the structures found for many oxide precipates in a metal matrix (Mader 1989, Kubawara, Spence and Rühle 1989), although in some metal–oxide systems similar 'incoherent' interfaces are observed (Mader 1989, Mushik 1989, private communication). It appears that for $\langle 100 \rangle_{Al}$ needles the correspondence cell is a hybrid of a conservative atom-by-atom correspondence along the needle axis $\langle 100 \rangle_{Al} \| \langle 110 \rangle_{Ge}$ with a near-CSL correspondence normal to the needle axis. {111} plate precipitates observe a similar hybrid correspondence with a near-CSL lattice in the habit plane and a one-to-one atomic correspondence normal to the habit (Westmacott and Dahmen 1987).

5.3. *Vacancies and twinning in the morphological development*

The relationships between different ORs, twinning and morphologies developed above can be used to paint a coherent picture of the growth of precipitates that unifies all the diverse observations made on this alloy system. The simplest OR is the cube–cube relationship illustrated in fig. 15. In Al–Si alloys it has been observed that, with this OR, precipitates form mainly plates on common {111} planes. This observation may be described by a vacancy–Ge atom coprecipitation mechanism advanced earlier. For plates to nucleate it is assumed that a high local vacancy concentration is necessary. This is because the plate must exceed a critical size before the associated Ge atoms can pucker into the diamond cubic structure. However, precipitate growth normal to this plane is difficult because the interstitial strain that builds up with every Ge layer is large and must be relieved periodically by the incorporation of vacancies. A similar mechanism can be postulated for {100} plates with the Bain correspondence. In the common {100} plane a one-to-one atomic correspondence with a small transformation strain allows for a good match. Furthermore, the OR in fig. 1 (*c*) ($100_{Al} \| 111_{Ge}$) might also nucleate by coprecipitation on $\{100\}_{Al}$. In each case, further precipitate growth occurs by a ledge mechanism, and the rate of growth will depend on the vacancy diffusion coefficient.

Fig. 17

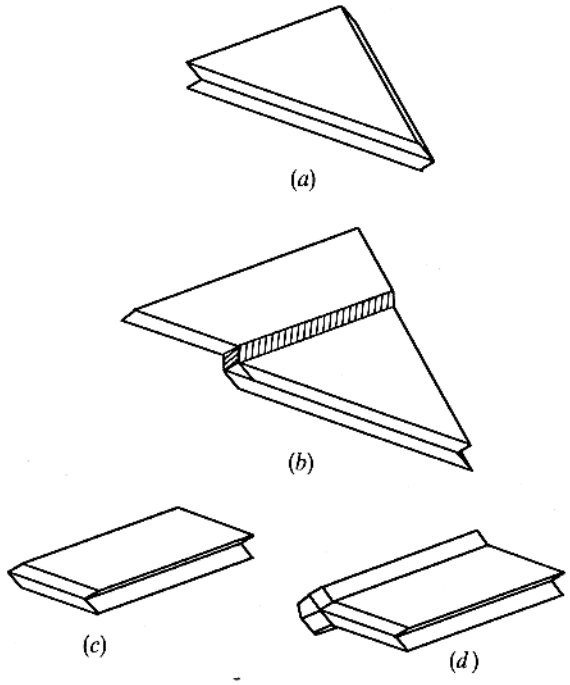

A {111} plate morphology is depicted for (*a*) a triangular twinned precipitate and (*b*) a subsequent twinning event that leaves its plate character unchanged. (*c*) An alternative morphology and further cozonal twinning that will lead to lath growth.

Plate growth for the cube–cube and the Bain correspondence is shown schematically in figs. 17 and 18 (*a*). The morphology on a {111} plane would be that of a hexagonal or triangular plate whereas that on a {100} plane would be a square or rectangular plate. An untwinned {100} plate in cross section would look like the particle in fig. 10. Twinning parallel to the habit plane without effect on the plate morphology is possible and has been seen only for {111} plates (Dahmen, Douin, Hetherington and Westmacott 1989). Such a twin parallel to the {111} habit plane is illustrated schematically in fig. 17 (*a*). For {111} plates this particular twin orientation is also favoured by the bias due to the shear component of the transformation strain.

If accidental twinning occurs on one of the other twin systems of the {111} plates, or on any twin system of the {100} plates, the lattice correspondence that is responsible for the plate shape will not be maintained. The plate morphology will be locally disturbed as shown in figs. 17 and 18 (*b*). Further growth of the twinned segment will be difficult, and it is likely that the next developing twin is one that reverts to the original orientation. This would lead to plates or laths such as that shown in fig. 9.

If the local vacancy concentration is low or if twinning occurs early in the growth of a precipitate, it is possible that other morphologies develop. This is illustrated schematically in figs. 17 and 18 (*c*). Once the first twin that destroys the high-symmetry OR necessary for plate growth has been formed, the only easy growth direction that remains from the original habit plane is the common ⟨110⟩ direction in fig. 18 and the $\langle 110\rangle_{Ge}$–$\langle 100\rangle_{Al}$ direction in fig. 17. Further twinning is now possible within the same $\langle 110\rangle_{Ge}$ zone without destroying the lattice match along the common growth

Fig. 18

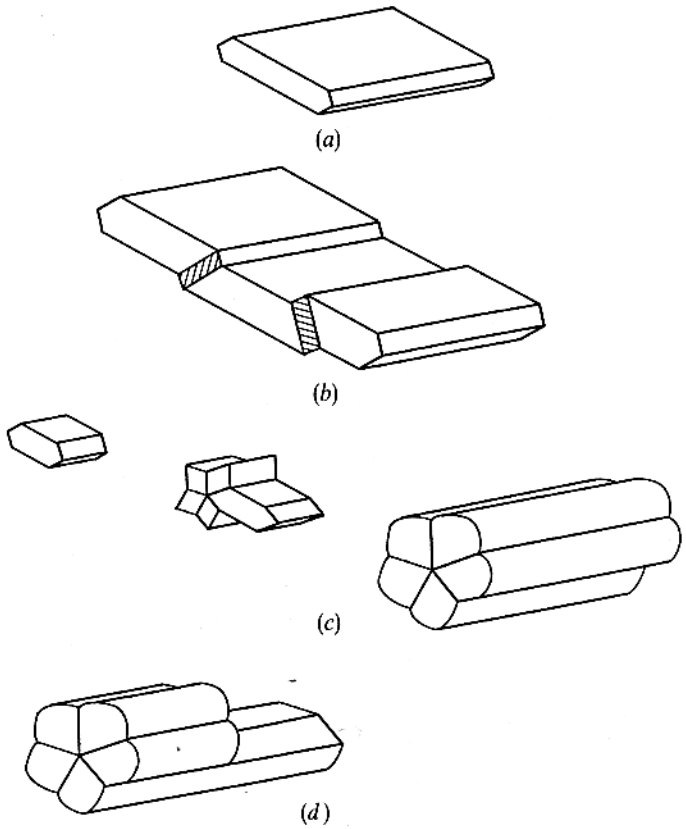

Schematic diagrams showing the various effects of twinning on a {100} plate morphology. In (*b*) the plate morphology is preserved, whereas in (*c*) and (*d*) needle morphologies are developed consistent with those observed experimentally.

direction. It is easy to see how only five distinct twin segments can be formed from each high-symmetry lattice correspondence and how their relative development depends on the sequence of twinning. During radial growth of these needles or laths vacancies can be added slowly as needed. The morphologies seeen in figs. 7–9, 11 and 12 can be rationalized in terms of such a sequence of events.

Finally, it is possible that during the lengthening of a needle or lath one or more of the original twin segments is discontinued, as shown schematically in fig. 18 (*d*). When such a needle is seen in cross-section, it will often show an irregular morphology and an irrational OR of the twin-related segments with the matrix. Such needles are seen in figs. 13 (*a*) and (*b*). The primary OR to which they are related by multiple twinning (inverse Bain correspondence) was found very infrequently and the possibility of plate growth on common {110} planes under conditions of high vacancy concentration, analogous to {111} and {100} plates for the cube–cube and Bain correspondences, has not been examined experimentally. However, it is likely that a similar transition from plates to laths or needles occurs for this case as well when the local vacancy concentration changes.

5.4. *Vacancies and twinning in nucleation*

In the preceding discussion, attention has been focused on understanding the morphologies that develop during precipitate growth in terms of accidental multiple twinning. A simple relationship between the precipitate type and the local vacancy concentration was hypothesized. The great variability of shapes and ORs were simply determined by different twinning sequences during growth. However, the role of twinning in the nucleation stage has not been addressed explicitly so far. Although in previous work (Westmacott and Dahmen 1987) a twinned nucleus for the case of $\langle 100 \rangle_{Al}$ needles was proposed, the possible function of twinning in the nucleation stage remains to be evaluated systematically.

In order to accommodate the large disparity in the atomic volumes of aluminium and germanium (16·6Å^3 as against 22·6 Å^3), precipitation and growth need an excess of vacancies, usually introduced by quenching (Russell 1969, Dahmen and Westmacott 1986b, Beller 1972). The ease of nucleation will be proportional to the concentration of vacancies. The lower the need a particular configuration has for vacancies, the more favoured the precipitation will be. Thus it is postulated that nucleation occurs by a process which tends to reduce the number of vacancies used by increasing the number of Ge–Ge bonds per atom for a given number of atoms per nucleus. The possible configurations that satisfy this condition in the diamond cubic structure can be constructed systematically. As shown in fig. 19, when the number of atoms involved is eight, ten or 12, special closed configurations, or cages, appear (fig. 20) in which the precipitate nucleus has a higher density.

The first complete nucleus with maximum density is the eight-atom cage drawn in fig. 20(*a*). As described by Angus and Hayman (1988) for the diamond structure, this nucleus consists mainly of six-membered rings with the so-called boat configuration and its extension will lead to a twinned crystal. This is not the case for the second cage in which ten atoms forming six-membered rings constitute the chair configuration known to give rise to an untwinned crystal (fig. 20(*b*)). The third configuration with 12 atoms (fig. 20(*c*)) is in fact the continuation of the first configuration with eight atoms, as the fourth is the next step after the ten-atom cage, and so on.

Fig. 19

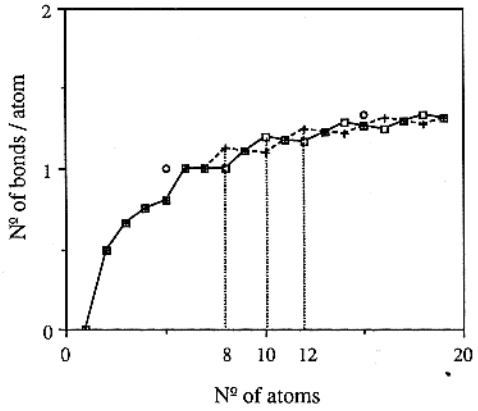

Plot of the variation in the number of bonds per atom in the diamond cubic structure as a function of cluster size for twinned (—+—) and untwinned (—□—) nuclei: (○), fivefold.

Fig. 20

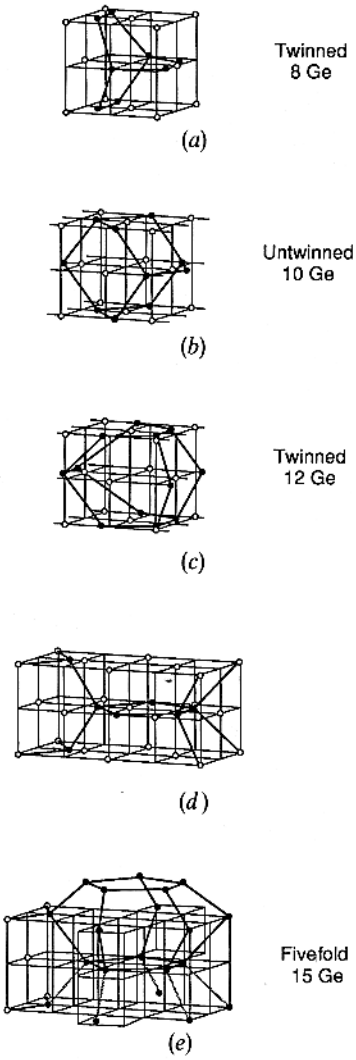

The different configurations indicated by the curve in fig. 19: (○), Al; (●), Ge. (*a*)–(*c*) first three cages; (*d*) related to the five-atom ring: (*e*) 15-atom cage related to the five-atom ring.

Since the precipitation occurs in the Al matrix, a nucleus is constrained by the condition of good match with the matrix. This match is illustrated for each nucleus configuration in fig. 21. Again, the twinned configuration appears more favourable since for a greater number of Ge atoms (14 against 12) in the same volume it needs one less vacancy.

It is clear from this discussion that twinning has a dual role in the formation of Ge precipitates in Al: during nucleation, it serves to maximize the number of Ge–Ge bonds and thus reduce the initial need for vacancies whereas, during growth, accidental twinning strongly influences the developing morphology.

Fig. 21

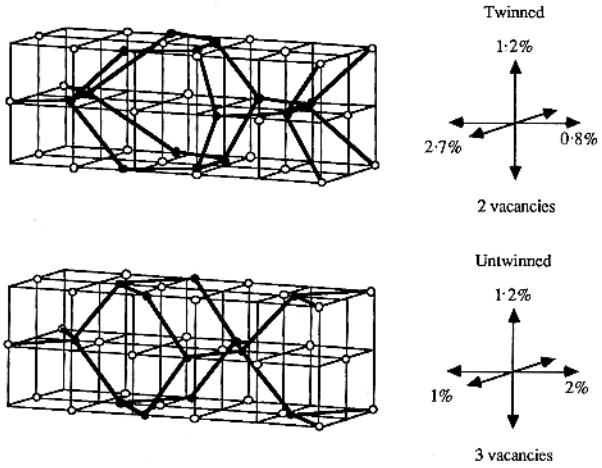

Complete unit cells corresponding to the two fundamental cages (figs. 20(*a*) and (*b*)); the mismatch between Ge precipitate and matrix as well as the number of vacancies required are indicated.

§6. Conclusions

The major results of the present study can be summarized as follows.

(1) Only a few different ORs and their twin derivatives are experimentally observed.
(2) Both $\langle 100\rangle_{Al}$ and $\langle 110\rangle_{Al}$ needle precipitates are usually twinned and the many different observed cross-section morphologies can be explained by the development of five cozonal twins in different proportions.
(3) All observed morphologies can be rationalized by different local vacancy concentrations and different sequences of multiple twinning.
(4) The predominant factors for the formation of the nucleus are the demand for vacancies and the minimization of the strain energy. The configuration which appears to follow these criteria best consists of only eight atoms and invariably leads to the formation of a twinned crystal.

Acknowledgments

We would like to thank C. Nelson for his assistance with the atomic-resolution microscopy and C. J. D. Hetherington for helpful comments on the manuscript. This work is supported by the Director, Office of Energy Research, Office of Basic Energy Sciences, Materials Sciences Division of the U.S. Department of Energy under Contract DE-AC03-76SF00098.

Note added in proof

It is interesting to note that in an early electron microscope study of silver bromide particles extensive multiple twinning was also observed (Hamilton and Brady 1964). In this work all the final particle shapes could be explained by accelerated growth at re-entrant twin junctions. The most important difference in the present work is the effect of the surrounding Al matrix and the OR adopted during nucleation. This reduces the symmetry to that of the bicrystal and may lead to the increased shape anisotropy. Most typical for this difference is the observation of {100} plates or laths as shown in fig. 10.

References

ANGUS, J. C., and HAYMAN, C. C., 1988, *Science*, **241,** 913.

BELLER, M., 1972, *Z. Metallk.*, **63,** 663.

CAHN, J. W., and KALONJI, G., 1981, *Proceedings of the International Conference on Solid–Solid Phase Transformations*, Pittsburgh, Pennsylvania, edited by H. I. Aaronson, D. E. Laughlin, R. F. Sekerka and C. M. Wayman (Pittsburgh: The Metallurgical Society of AIME), p. 3.

DAHMEN, U., DOUIN, J., HETHERINGTON, C. J. D., and WESTMACOTT, K. H., 1989, *Materials Research Society Symposium Proceedings*, Vol. 139, edited by W. Krakow, F. A. Ponce and D. J. Smith (Pittsburgh, Pennsylvania: Materials Research Society), p. 87.

DAHMEN, U., NELSON, C., and WESTMACOTT, K. H., 1986, *Proceedings of the 44th Annual Meeting of the Electron Microscopy Society of America*, edited by G. W. Bailey (San Francisco, California: San Francisco Press), p. 538.

DAHMEN, U., PELTON, A. R., WITCOMB, M. J., and WESTMACOTT, K. H., 1981, *Proceedings of the International Conference on Solid Phase Transformations*, Pittsburgh, Pennsylvania, edited by H. I. Aaronson, D. E. Laughlin, R. F. Sekerka and C. M. Wayman (Pittsburgh, The Metallurgical Society of AIME), p. 637.

DAHMEN, U., and WESTMACOTT, K. H., 1986a, *Science*, **233,** 875; 1986b, *Materials Research Society Symposium Proceedings*, Vol. 62, edited by L. W. Hobbs, K. H. Westmacott and D. B. Williams; (Pittsburgh, Pennsylvania: Materials Research Society), p. 217; 1989, *J. Electron Microsc. Technique* (submitted).

D'ANTERROCHES, C., and BOURRET, A., 1984, *Phil. Mag.* A, **49,** 783.

GAO, Y., SHEWMON, P., and DREGIA, S. A., 1988, *Scripta metall.*, **22,** 1521.

GOUTHAMA, G. N., SUBBANNA and KISHORE, 1985, *Mater. Sci. Forum*, **3,** 261.

GOUTHAMA, G. N., and KISHORE, 1987, *Proceedings of the Conference on Phase Transformations*, edited by G. W. Lorimer (London, The Institute of Metals), , p. 551.

HAMILTON, J. F., and BRADY, L. E., 1964, *J. appl. Phys.*, **35,** 414.

HEINEMANN, K., YACAMÁN, M. J., YANG, C. Y., and POPPA, H., 1979, *J. Cryst. Growth*, **47,** 177.

HUGO, G. R., and MUDDLE, B. C., 1986, Research Report, Monash University; 1989, *Acta Metall. Mater.*, **38,** 351, 365.

IIJIMA, S., 1987, *Jap. J. appl. Phys.*, **26,** 357, 365.

INO, S., 1966, *J. Phys. Soc. Japan*, **21,** 346; 1969, *Ibid.* **27,** 941.

JEFFERSON, D. A., and KIRKLAND, A. I., 1988, *Proceedings of the Institute of Physics Short Meeting on Electron Beam Imaging of Non-Crystalline Materials, London*, edited by K. Knowles (Bristol: Institute of Physics), p.71.

KOBAYASHI, K., SHINGU, P. H., and OZAKI, R., 1976, *J. Mater. Sci.*, **11,** 399.

KÖSTER, U., 1969, *Mater. Sci. Engng.*, **5,** 174; 1971, Ph.D. Thesis, Göttingen.

KUWABARA, M., SPENCE, J. C. H., and RÜHLE, M., 1989, *J. Mater. Res.*, **4,** 972.

LI, Y., and GUO, K., 1985, *Proceedings of the Third Chinese–Japanese Electron Microscopy Seminar*, Hanzhou, edited by H. Hashimoto, K. H. Kuo, L. Lee and K. Ogawa, p. 71.

LORIMER, G. W., and NICHOLSON, R. B., 1969, *Institute of Metals Monograph*, Vol. 33 (London: Institute of Metals), p. 36.

LU, S. Z., and HELLAWELL, A., 1987, *Metall. Trans.* A, **18,** 1721.

MADER, W., 1989, *Z. Metallk.*, **80,** 139.

MARKS, L. D., 1984, *Phil. Mag.* A, **49,** 81.

MATSUMOTO, S., and MATSUI, Y., 1983, *J. Mater. Sci.*, **18,** 1785.

OZAWA, E., and KIMURA, H., 1970, *Acta metall.*, **18,** 995.

ROSENBAUM, H. S., and TURNBULL, D., 1958, *Acta metall.*, **6,** 653; 1959,

RUSSELL, K. C., 1969, *Scripta metall.*, **3,** 313.

SAULNIER, A., 1961, *Mem. scient. Revue. métall.*, **58,** 615.

SKROTZKI, W., WENDT, H., CARTER, C. B., and KOHLSTEDT, D. L., 1988, *Phil. Mag.* A, **57,** 383.

WESTMACOTT, K. H., and DAHMEN, U., 1982, *Proceedings of the 40th Annual Meeting of the Electron Microscopy Society of America*, Washington, DC, edited by G. W. Bailey (San Francisco, California: San Francisco Press), p. 62a; 1985, *Mater. Sci. Forum*, **3,** 325; 1986, *Rev. Phys. Appl.*, **21,** 757; 1987, *Proceedings of the Conference on Phase Transformations*, Cambridge, edited by G. W. Lorimar (London, The Institute of Metals), p. 357.

ZUR, A., and MCGILL, T. C., 1983, *J. appl. Phys.*, **55,** 378.